Cardiovasc Intervent Radiol (2019) 42:250–259
https://doi.org/10.1007/s00270-018-2096-8

CLINICAL INVESTIGATION IMAGING

Arterial Phase CTA Replacement by a Virtual Arterial Phase Reconstruction from a Venous Phase CTA: Preliminary Results Using Detector-Based Spectral CT

Anish A. Patel[1] · Patrick D. Sutphin[1] · Yin Xi[1] · Suhny Abbara[1] · Sanjeeva P. Kalva[1]

Received: 7 May 2018 / Accepted: 12 October 2018 / Published online: 24 October 2018

Abstract
Objective To assess the feasibility of creating virtual monoenergetic arterial images from venous phase CTA obtained on a detector-based spectral CT scanner and quantitatively compare the signal-to-noise (SNR) and contrast-to-noise (CNR) ratios of the major arteries to those on polyenergetic true arterial phase images.
Methods In this retrospective study, 23 patients (15 men and 8 women, median age 68 years) who underwent triple-phase CTA on a spectral CT scanner for aortic endograft surveillance were included. The venous phase CTA of each study was reconstructed to generate virtual monoenergetic images at various keV, which were compared to true arterial phase CTA images. SNR and CNR of the aortoiliac arteries were evaluated by testing the differences in means and non-inferiority of virtual arterial images to true arterial images. Effective radiation dose was calculated for standard triple-phase studies in comparison with dual-phase and single-phase spectral CT examinations.
Results Virtual monoenergetic images demonstrated non-inferior ($P < 0.05$) arterial SNR and CNR compared to true arterial images at 40 keV for all arteries, at 45–50 keV for the thoracic and suprarenal aorta, and at 45–55 keV for the infrarenal aorta and iliac arteries. Significantly higher ($P < 0.05$) arterial attenuation was obtained at 40 keV for the aortoiliac arteries. Mean effective dose for conventional triple-phase studies was 32.5 mSv in comparison with 21.3 mSv for dual-phase non-contrast/venous scans and 11.3 mSv for single-phase venous scans.
Conclusions Detector-based spectral CT enables creation of virtual monoenergetic arterial images from venous phase CTA with equivalent and in some cases significantly higher SNR/CNR of major arteries compared to images from true arterial phase polyenergetic CTA.

Keywords CT angiography · Spectral CT · Dual-energy CT · Aorta

Advances in Knowledge

- Spectral detector CT (SDCT) technology separates emitted X-rays at the detector level, unlike dual-energy CT (DECT) which does so at the source level, allowing for retrospective spectral analysis at 120 or 140 kVp without requiring separate protocols or further radiation exposure.
- SDCT has the ability to generate virtual monoenergetic images by scaling attenuation from discrete energy levels, which enables vessels to be retrospectively enhanced or de-enhanced while reducing nearby streak and beam hardening artifacts.
- Virtual monoenergetic arterial images derived from a venous phase CT have equivalent and in some cases significantly higher SNR/CNR than the true arterial phase images for central thoracic and visceral arteries.

✉ Anish A. Patel
anish.patel@phhs.org

[1] Department of Radiology, University of Texas Southwestern Medical Center, 5323 Harry Hines Boulevard, Dallas, TX 75390, USA

Implications for Patient Care

1. Virtual arterial imaging using SDCT may allow for the elimination of the arterial phase in conventional triple-phase studies, which would decrease overall patient radiation exposure due to fewer acquisitions.
2. Additionally, retrospective vascular enhancement using SDCT may salvage scans with suboptimal contrast bolus timing and allow for lower contrast volumes without compromising image quality.

Introduction

Although dual-energy CT (DECT) has attained mainstream clinical use relatively recently, newer methods for spectral discrimination are still being developed. DECT allows emission of polyenergetic X-rays at two different kilovolt potentials (kVp) using a dual-source or rapid kVp switching method. Spectral detector CT (SDCT) technology utilizes two layers of different scintillating crystals with their own photodiode detectors. Low- and high-energy photons from the polyenergetic X-ray beam are differentially absorbed in a yttrium-based detector as well as a second, thicker gadolinium-based detector, after which the incoming photons are sorted into different energy bins using pulse height discrimination [1, 2]. The raw data are decomposed with full temporo-spatial registration based on light–matter interactions such as the photoelectric effect and Compton scattering. SDCT acquisition thus allows for retrospective spectral analysis without requiring separate protocols or further radiation exposure [3]. Energy-resolving photon-counting detectors such as SCDT offer other advantages over DECT such as more robust spectral separation, with an estimated 30% improvement in geometric efficiency over conventional energy-integrating detectors [2].

Among a multitude of potential clinical applications, SDCT has ability to create virtual monoenergetic (VME) images generated by scaling attenuation from discrete energy levels ranging from 40 to 200 kiloelectron volts (keV). This has considerable utility in vascular imaging since vessels can be retrospectively enhanced or de-enhanced while reducing nearby streak and beam hardening artifacts. Similar to DECT, the lower end of the virtual monoenergetic range is particularly useful in increasing vascular enhancement as these images are more influenced by the photoelectric effect and since the attenuation of iodine is optimal just above its k shell binding energy of 33 keV [4]. Since contrast produces higher attenuation at the lower keV ranges near the k edge of iodine, higher SNR can be achieved by weighting monoenergetic images to these lower levels. Therefore, attenuation from the small amount of arterial contrast present during the venous phase is increased relative to background, and vessels therefore appear more enhanced. Given that arterial signal from a venous phase study is artificially increased in a retrospective fashion, a "virtual" image with arterial enhancement is created [4, 5]. Conversely, at higher keV, the image quality is more heavily affected by Compton scatter and less susceptible to beam hardening artifacts compared to polyenergetic beams [2, 3, 6].

Previous studies demonstrate that monoenergetic images from DECT improve image quality of the pre- and post-operative aorta [6–16] as well as the visceral [6, 17–19] and peripheral [20, 21] vasculature compared to conventional single-source polyenergetic CT angiography (CTA). While these studies explored the use of DECT in CTA, the literature is sparse with respect to the newer SDCT technology due to its incipient introduction into clinical use. The purpose of this study was to assess the feasibility of creating virtual monoenergetic arterial images from venous phase CTA obtained on a detector-based spectral CT scanner and quantitatively compare the signal-to-noise (SNR) and contrast-to-noise (CNR) ratios of the major arteries on these images to those on the polyenergetic true arterial phase images.

Materials and Methods

Patient Selection

For this IRB-approved and HIPAA compliant study, a written informed consent was obtained from all patients. Any patients younger than 18 years old, pregnant, or with contraindications to iodinated contrast material were excluded. From August 2015 to December 2016, 351 outpatients underwent a clinically indicated CT examination on a prototype SDCT scanner (IQon, Philips Healthcare). Of these, 23 consecutive patients (15 men (mean age 66 years, age range 49–87 years) and 8 women (mean age 67 years, age range 52–78 years)) who underwent surveillance CTA following endovascular aortic repair were included in this study. The venous phase acquisition of the triple-phase (arterial, delayed venous, and non-contrast) CTA study was reconstructed to generate virtual monoenergetic image dataset to be compared to the true arterial phase CTA.

CT Technique

Examinations were chosen for aortic stent graft evaluation and were standardized into chest, abdomen/pelvis, or most commonly combined chest/abdomen/pelvis protocols.

Chest studies extended from the lower neck to the upper abdomen, while abdominopelvic studies extended from the diaphragm to the bottom of the femoral heads. Patients were positioned supine and feet-first. All patients underwent unenhanced imaging prior to contrast administration, which was performed in the arterial and delayed (90 s) phases using bolus tracking software. Isovue 370 (Bracco Diagnostics Inc, Princeton, NJ) was administered via a 20-gauge or larger intravenous catheter in the antecubital fossa or forearm at a rate of 4 mL/s for a total of 120 mL. A tube potential of 120 kVp was used and configured for 64 × 0.625 mm collimation with pitch 1.71. An amperage setting of 73–214 mAs was used, and automatic tube current modulation was employed. Gantry rotation time was 0.4 s, and slice thickness was set at 2 mm with 1-mm intervals.

Dose reduction techniques for the SDCT were the same as for single-energy scanners from the same manufacturer, and the protocols were thus identical, using automatic exposure control in all three planes. Image reconstruction for this scanner can either utilize data from both detector layers to create conventional CT images or data from each layer separately to create spectral base images. In this study, images for the true arterial (120 kVp) phase were created using the conventional reconstruction as a reference while virtual arterial images were reconstructed from the venous phase spectral base images to generate monoenergetic image data from 40 to 70 keV at 5-keV intervals (Fig. 1). In our SDCT scanner, 70 keV images are the equivalent of conventional polyenergetic 120 kVp images, resulting in similar attenuation values for adult body scans [3]. Therefore, monoenergetic images beyond 70 keV were not evaluated as they were not expected to show sufficient vessel attenuation. Primary axial images were reconstructed in 0.5-mm slices with additional 2 mm axial, sagittal, and coronal reconstructions.

Quantitative Image Analysis

Image analysis was performed on an independent workstation (thin-client Spectral Diagnostic Suite of applications, Philips Healthcare). The two image sets (true arterial phase CTA and virtual monoenergetic image data from venous phase CTA) were automatically co-registered and analyzed side by side. Multiple circular regions of interest (ROI) were manually placed in the following vessels: bilateral carotid arteries, bilateral subclavian arteries, brachiocephalic artery, aorta (ascending, arch, descending, suprarenal, infrarenal), celiac artery, superior mesenteric artery, bilateral renal arteries, bilateral common iliac arteries, and bilateral external iliac arteries. The ROIs were drawn to fill the luminal diameter for each vessel with care taken to avoid the vessel wall, atherosclerotic plaques, calcifications, and metallic stent material. In cases of dissection, measurements were made in the true lumen. Completely thrombosed and severely stenotic vessels rendering accurate ROI measurement impossible were excluded. ROIs were first placed on the conventional true arterial images and then copied to each of the virtual monoenergetic images using the copy/paste function in the software, with manual adjustments for minor differences in respiration between the acquisitions as needed. For each ROI, average attenuation in Hounsfield units (HU) and onefold standard deviation (SD) was recorded.

Using these measurements, the signal-to-noise ratio (SNR) for each segment was determined using the following equation where ROI_{vessel} indicates the average attenuation for the vessel of interest and ROI_{SD} denotes the standard deviation: $SNR = ROI_{vessel}/ROI_{SD}$. The SNR calculation allowed for the evaluation of intravascular enhancement to determine the homogeneity of contrast within the vessels, given that optimally enhanced vessels would be expected to show low signal fluctuation. To independently assess image contrast in the setting of extravascular noise, 1-cm^2 circular ROIs were drawn in the axillary fat, peri-celiac fat, mesenteric fat, and psoas fat. This contrast-to-noise ratio (CNR) was calculated as: $CNR = (ROI_{vessel} - ROI_{fat})/(ROI_{noise})$, where ROI_{fat} is average fat attenuation and ROI_{noise} is the SD of the fat attenuation. These two matrices of SNR and CNR were calculated to evaluate the image quality at each location.

Statistical Methods

Repeated measure analysis of variance (ANOVA) models were used to test the difference in means of the virtual arterial phase at each energy level to the true arterial phase for each region of interest, respectively. Heteroskedasticity (changing variation across energy levels) was accounted for by allowing different covariance matrix for each energy level. One-side multiple pair-wise comparisons with Dunnett correction were used to test whether virtual arterial phase at each energy level had higher mean SNR/CNR than that of the true arterial phase. Similar models were used for testing the non-inferiority of virtual arterial phases to the true arterial phase. The null hypotheses were the virtual monoenergetic images that had mean SNR/CNR at least 5 units less than that of the true arterial phase (inferiority margin of 5 SNR/CNR) images, in keeping with cutoffs in other studies examining the non-inferiority of SNR and CNR between imaging techniques [22].

Radiation Dose Calculation

For each patient, effective dose for each study was calculated in millisieverts (mSv) by multiplying the dose-length

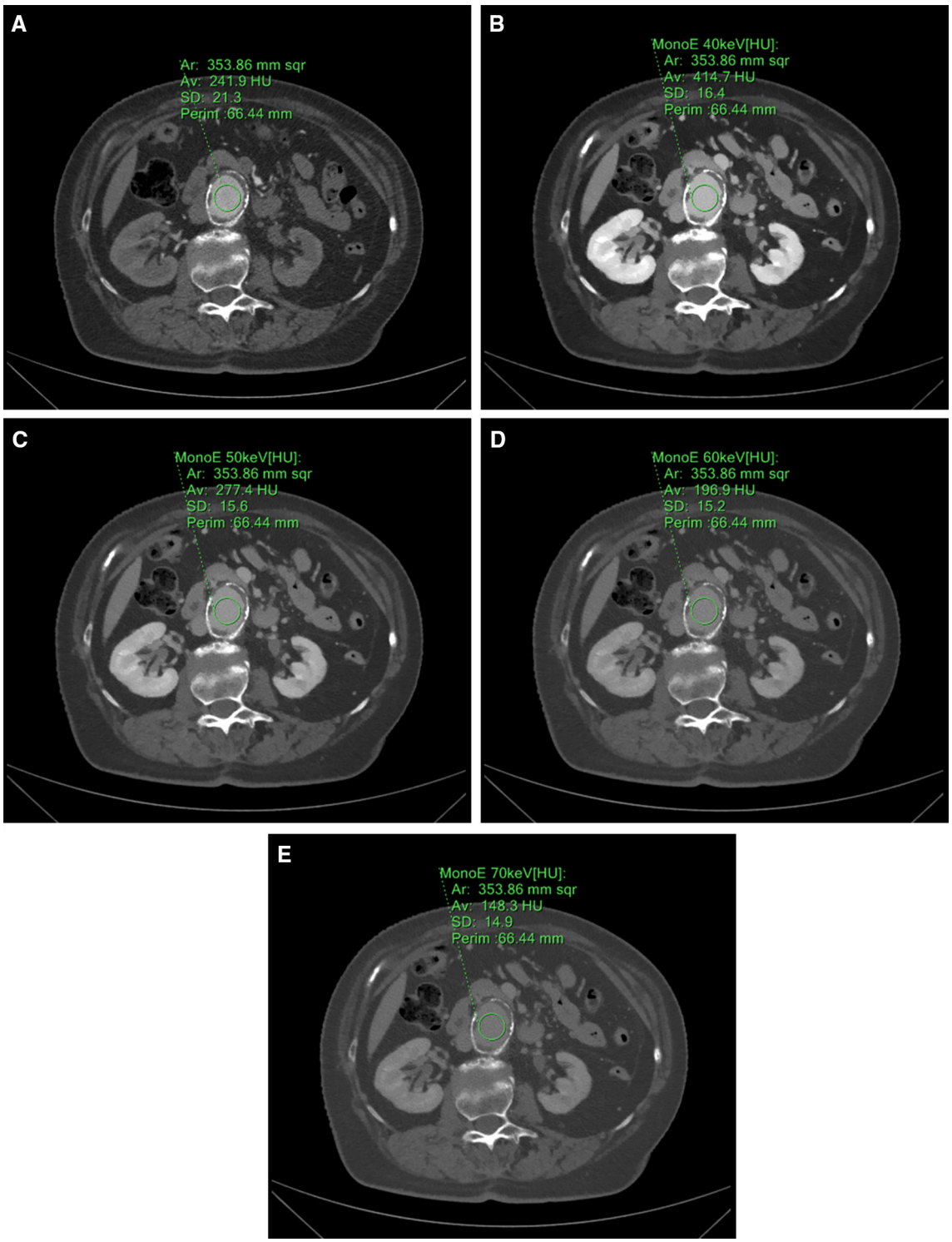

Fig. 1 Identical circular ROI drawn on true arterial (**A**) and virtual monoenergetic arterial images at 40 keV (**B**), 50 keV (**C**), 60 keV (**D**), and 70 keV (**E**) within the lumen of the aorta at the level of the kidneys. Data displayed includes mean attenuation in HU and standard deviation

product (DLP, in milligray) by an overall tissue-weighting factor (k), which normalizes effective dose over certain body regions [9]. In our study, utilizing CTA of the chest, abdomen, and pelvis, k used to approximate patient dose was 0.019 mSv/mGy/cm [23].

Results

A total of 391 vessel segments were evaluated. Of these, 107 had endovascular stents, 19 had unstented aneurysms, and 35 had dissected lumens. No endoleaks were identified on true or virtual arterial images. Between the true arterial images and the set of virtual monoenergetic images, 4329 ROIs were measured and analyzed across all patients. Both SNR and CNR demonstrated an inverse correlation with keV levels, reaching a maximum at 40 keV with a mean SNR for virtual monoenergetic arterial images of 22.7 ± 4.8 compared to a true arterial mean 18.5 ± 4.9 (123% relative increase). The mean CNR for virtual monoenergetic arterial images was 41.2 ± 6.2 compared to a true arterial mean 32.8 ± 6.3 (126% relative increase). Graphs comparing mean attenuation of virtual monoenergetic and true arterial images are shown in Fig. 2. For each arterial segment at each energy level, testing for both non-inferiority and significant differences was performed to compare SNR and CNR between virtual monoenergetic and true arterial images. The virtual monoenergetic images demonstrated arterial contrast attenuation that is non-inferior to true arterial phase images at 40 keV for all investigated vessels, at 45–50 keV for the thoracic and suprarenal abdominal aorta and at 45–55 keV for the infrarenal aorta and iliac arteries. Significantly higher arterial attenuation was obtained at 40 keV for the entire aorta and iliac arteries (Fig. 3).

Non-inferiority Testing

Summary tables comparing the non-inferiority of virtual monoenergetic images to true arterial phase images for both SNR and CNR can be found in Tables 1 and 2. The SNR and CNR in the virtual monoenergetic images were found to be statistically ($P < 0.05$) non-inferior to those of the true arterial images at energy levels up to 55 keV. At 40 keV, all evaluated arterial locations were found to be non-inferior when using CNR and all locations except the right subclavian and brachiocephalic arteries were non-inferior using SNR. At 50 keV, the entire aorta, iliac arteries, and mesenteric branch vessels were non-inferior using SNR and only the distal aorta and iliac arteries were non-inferior using CNR.

Difference Testing

Summary tables comparing the one side test of difference between virtual monoenergetic images and true arterial phase images for both SNR and CNR can be found in Tables 3 and 4. The CNR and SNR in the virtual monoenergetic images were found to be significantly ($P < 0.05$) higher than those of the true arterial images at 40 and 45 keV. These locations were predominantly the multilevel aorta, common iliac arteries, and external iliac arteries.

Radiation Dose Reduction

For the conventional triple-phase study (non-contrast, arterial phase, and venous phase), mean effective radiation dose among all patients was 32.5 mSv. After excluding the dose from the arterial phase, mean radiation dose for dual-phase non-contrast and venous phase scans was 21.3 mSv (35% reduction) and single-phase venous scans was 11.3 mSv (65% reduction).

Discussion

Although virtual monoenergetic vascular imaging has been studied using DECT, to our knowledge this is the first study to directly compare SDCT-based venous phase virtual monoenergetic images to true arterial images using objective image quality indices. The SDCT virtual monoenergetic images from venous phase CTA were at least equivalent to conventional arterial images at lower keV and have significantly higher contrast attenuation in more distal arteries, potentially due to a variation in contrast timing or decreased image noise from lessened soft tissue mass [20]. Our results suggest that 40 keV provides ideal vascular contrast, in agreement with prior DECT studies examining noise-optimized image-based virtual monoenergetic algorithms compared to traditional virtual monoenergetic techniques, likely due to similar noise reduction software in the SDCT scanner [7, 17, 21]. Energies below 35 keV would fall under the k edge of iodine and are insufficient in providing adequate enhancement. A polyenergetic beam with low kVp would be suboptimal since the wide range of keV from the spectrum of energies would result in energies too far above and below the iodine k edge, reducing attenuation. As a result, narrow monoenergetic beams centering at specific keV rather than broad conventional polyenergetic beams are better suited to target the desired energy around the k edge of iodine.

These findings are concordant with similar studies evaluating DECT that show increased intravascular enhancement at low keV levels as they approach the k edge of iodine at 33 keV, raising the possibility for a reduced contrast bolus which has been suggested in many studies examining DECT virtual monoenergetic imaging [2, 6, 7, 16–18, 20, 21]. Early SDCT research for cardiac imaging in patients being evaluated for aortic valve replacement has also shown that virtual monoenergetic

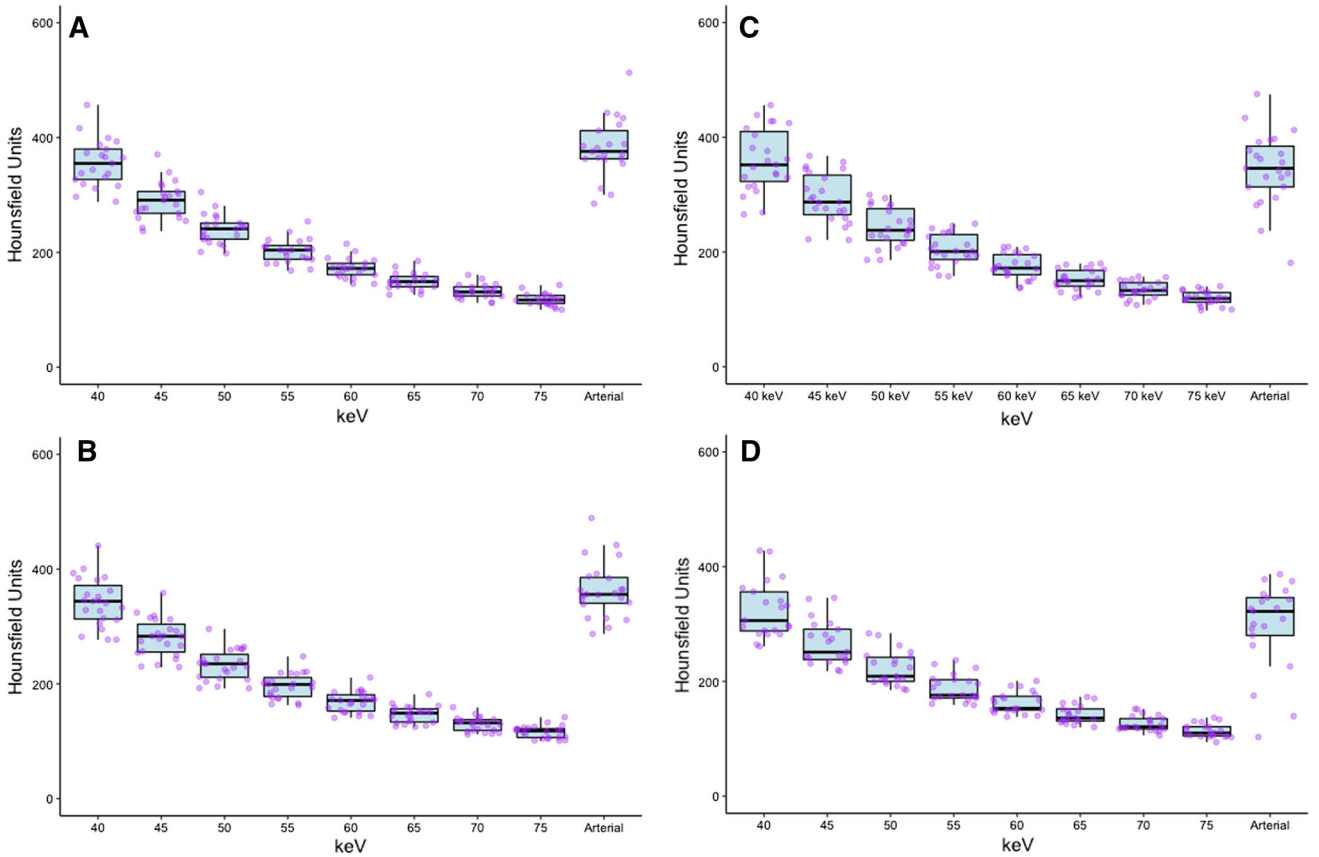

Fig. 2 Box and scatter plots comparing mean attenuation and standard deviation of virtual monoenergetic arterial images at increasing keV levels to those of true arterial images on the far right. Data from the aortic arch (**A**), suprarenal abdominal aorta (**B**), infrarenal abdominal aorta (**C**), and right external iliac artery (**D**) are shown as examples

imaging allows for lower contrast material volumes without compromising image quality or increasing radiation exposure [3]. A decreased volume of intravenous contrast material may be of particular utility in many patients who often have an associated renal dysfunction.

Furthermore, our study suggests that the arterial phase CT may be eliminated from traditional triple-phase CTAs with spectral CT imaging, given that monoenergetic spectral CTA data from a venous phase CT has similar arterial enhancement to that of true arterial phase CT data. The notion of replacing the arterial phase by an equivalent virtual arterial phase has received particular attention in recent years with DECT. Many patients requiring vascular imaging such as for endovascular surveillance undergo decades worth of CTAs, dramatically increasing lifetime radiation exposure. The established literature for DECT has shown that routine aortic CTAs and aortic endograft CTAs have the potential to reduce radiation exposure using venous phase virtual monoenergetic images by eliminating the arterial phase, without compromising image quality [7, 9, 12, 14, 15, 17, 18]. Using techniques similar to prior studies examining DECT, we found comparable radiation dose reduction in SDCT. Approximately 35% dose reduction is achievable by replacing the true arterial phase with virtual arterial images. Additionally, since virtual non-contrast images can also be produced by spectral CT, single-phase venous scans can be performed and would allow for up to 65% total radiation dose reduction. However, additional prospective studies are needed to evaluate the potential for reduced radiation exposure as well as contrast dosing in the setting of fewer phases, as well as to directly compare SDCT virtual monoenergetic imaging to that of established DECT technology.

One potential disadvantage of a single-phase acquisition is the absence of dynamic information that can be seen with multiphase scans, such as localizing the precise source of contrast extravasation in endoleaks. However, several studies examining DECT have indicated that delayed or late delayed imaging may be more sensitive than the arterial phase for aortic endograft surveillance, given that low-flow endoleaks may not be apparent initially [9–12]. As our study did not directly examine these contexts, similar research will need to be conducted for virtual monoenergetic imaging using spectral CT, including potential additional studies where a virtual arterial phase may sufficiently replace a true arterial phase such as for

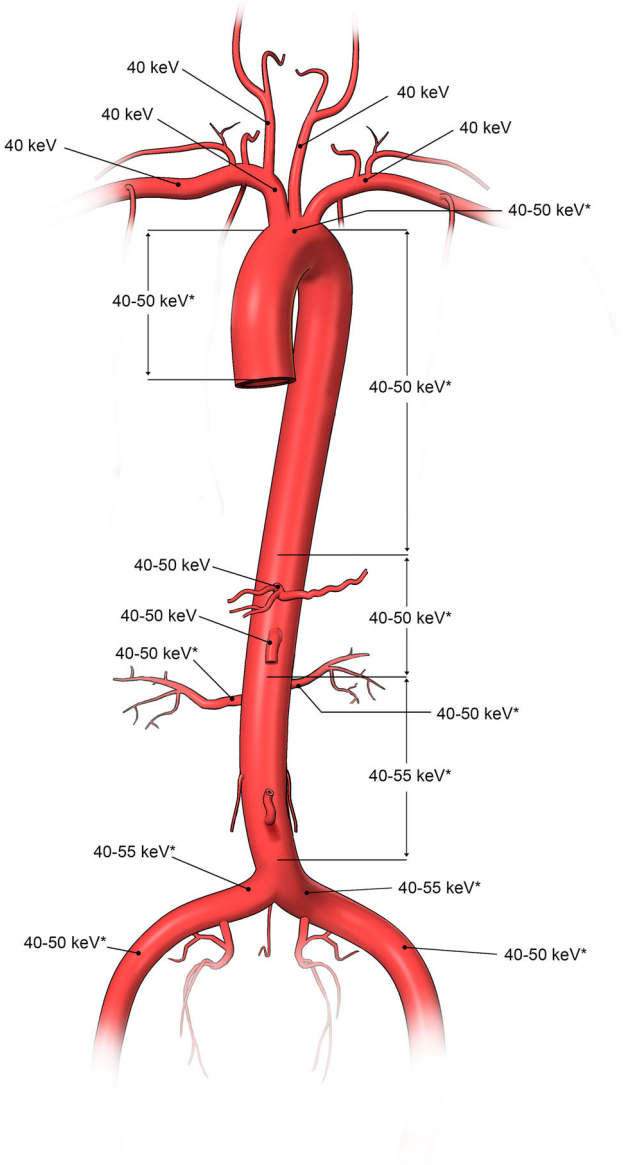

Fig. 3 Range of virtual monoenergetic arterial keV values non-inferior to arterial phase images at each location. Asterisk indicates significantly higher SNR or CNR for at least 40 keV

detecting active extravasation in vascular injury. A further advantage of low-energy monoenergetic imaging with spectral CT is the ability to perform retrospective vascular enhancement in the setting of suboptimal contrast timing, which is one of the most common reasons for diagnostic failure in conventional CT angiography [6].

An important advantage of SDCT technology over DECT lies in its ability to retrospectively create spectral images without the need for selecting patients beforehand [3]. Because spectral data is acquired at the detector level instead of the X-ray tube, all studies scanned at 120 or 140 kVp allow for spectral separation. This can simplify imaging protocols and enable retrospective enhancement in case of poor contrast timing or characterization for incidental findings. The spectral base image (SBI) data created by the technology at the scanner console is sent to the radiologist workstation for post-processing and enables reconstruction within seconds [1]. In addition to virtual monoenergetic vascular enhancement, other applications not discussed in this paper such as virtual non-contrast imaging, iodine mapping, material decomposition, and artifact reduction can be performed on demand without special protocols. Unlike DECT, SDCT has no field of view, cross-scatter, or gantry rotation time limitations [3].

A number of limitations to our preliminary study must be considered. First, we evaluated a relatively small patient cohort in a retrospective fashion, measuring only quantitative image parameters as a surrogate for image quality. Observer-based qualitative image analysis and prospective assessment of diagnostic outcomes will need to be performed for more robust clinical applicability. Specific studies are also needed to evaluate the potential for reduced contrast material dosage and radiation exposure in the setting of fewer contrast phases, as well as to directly compare SDCT virtual monoenergetic imaging to that of DECT. Additionally, because the fraction of vessels affected by significant streak artifact from contrast material boluses, calcifications, and metallic stents was relatively low, subgroup analysis was not performed for these segments. Specific evaluation to account for streak artifact may be helpful in explaining the minor discrepancy in which the SNRs of right subclavian and brachiocephalic arteries on virtual monoenergetic images were not found to be non-inferior compared to that on the true arterial images, since a dense contrast bolus is often present in these locations. Optimal keV for areas heavily affected by streak artifact is likely to be higher due to the reduction in streak artifact at increasing monoenergetic levels, as suggested by DECT studies evaluating virtual monoenergetic imaging for endovascular stent surveillance [8–10, 12]. Given the ability of SDCT to reconstruct the CT data at multiple keV levels, metal artifacts can be reduced by reconstructing an additional data set at 70 or 80 keV [8]. A follow-up study focused on streak artifact reduction by spectral CT in the setting of CT angiography would be ideal. Along similar lines, optimal keV may vary slightly due to image noise secondary to patient BMI and locations in the body with comparatively little surrounding soft tissues, such as in the limbs [20]. Finally, due to limited commercial availability, these results are also only valid for the CT system and post-processing software of a single vendor.

Table 1 *P* values depicting non-inferiority of virtual monoenergetic arterial images compared to true arterial phase images using SNR

Arterial segment	40 keV	45 keV	50 keV	55 keV
Venous phase monoenergy values with non-inferior SNR compared to arterial phase				
R carotid	0.04	0.28	0.68	1
L carotid	0.02	0.13	0.52	0.91
R subclavian	0.21	0.59	0.88	1
L subclavian	0.004	0.01	0.09	0.38
Brachiocephalic	0.23	0.70	1	1
Asc thoracic aorta	< 0.001	< 0.001	0.01	0.33
Aortic arch	< 0.001	< 0.001	0.04	0.48
Desc thoracic aorta	< 0.001	< 0.001	0.03	0.46
Suprarenal aorta	< 0.001	< 0.001	0.01	0.26
Celiac	< 0.001	< 0.001	0.00	0.06
Superior mesenteric	< 0.001	< 0.001	0.03	0.32
R renal	< 0.001	< 0.001	0.00	0.03
L renal	< 0.001	< 0.001	0.01	0.13
Infrarenal aorta	< 0.001	< 0.001	0.001	0.04
R common iliac	< 0.001	< 0.001	< 0.001	0.01
L common iliac	< 0.001	< 0.001	< 0.001	0.01
R external iliac	< 0.001	< 0.001	0.01	0.14
L external iliac	< 0.001	< 0.001	0.01	0.10

All *P* values at 60 keV and beyond were statistically insignificant and excluded from the table

Table 2 *P* values depicting non-inferiority of virtual monoenergetic arterial images compared to true arterial phase images using CNR

Arterial segment	40 keV	45 keV	50 keV	55 keV
Venous phase monoenergy values with non-inferior CNR compared to arterial phase				
R carotid	0.01	0.15	0.47	0.91
L carotid	0.02	0.19	0.51	0.86
R subclavian	0.01	0.10	0.35	0.78
L subclavian	0.004	0.08	0.32	0.75
Brachiocephalic	0.004	0.10	0.42	0.85
Asc thoracic aorta	0.002	0.04	0.27	0.75
Aortic arch	< 0.001	0.02	0.16	0.63
Desc thoracic aorta	0.001	0.07	0.63	1
Suprarenal aorta	0.001	0.06	0.60	1
Celiac	0.003	0.12	0.67	1
Superior mesenteric	0.002	0.12	0.72	1
R renal	< 0.001	0.02	0.26	0.92
L renal	0.009	0.15	0.64	1
Infrarenal aorta	< 0.001	< 0.001	0.001	0.07
R common iliac	< 0.001	< 0.001	< 0.001	0.01
L common iliac	< 0.001	< 0.001	< 0.001	0.00
R external iliac	< 0.001	< 0.001	< 0.001	0.01
L external iliac	< 0.001	< 0.001	< 0.001	0.00

All *P* values at 60 keV and beyond were statistically insignificant and excluded from the table

Table 3 *P* values depicting virtual monoenergetic arterial images with significantly higher SNR compared to true arterial phase images

Arterial segment	40 keV	45 keV	50 keV	55 keV
Venous phase monoenergy values with significantly higher SNR compared to arterial phase				
R carotid	0.61	0.94	1	1
L carotid	0.38	0.87	1	1
R subclavian	0.95	1	1	1
L subclavian	0.48	0.87	1	1
Brachiocephalic	0.75	1	1	1
Asc thoracic aorta	0.00	0.07	0.80	1
Aortic arch	0.03	0.40	1	1
Desc thoracic aorta	0.01	0.28	1	1
Suprarenal aorta	0.02	0.53	1	1
Celiac	0.05	0.68	1	1
Superior mesenteric	0.06	0.71	1	1
R renal	0.03	0.50	1	1
L renal	0.04	0.58	1	1
Infrarenal aorta	0.00	0.21	1	1
R common iliac	0.00	0.02	0.63	1
L common iliac	0.00	0.04	0.57	1
R external iliac	0.01	0.23	0.82	1
L external iliac	0.01	0.10	0.62	1

All *P* values at 60 keV and beyond were statistically insignificant and excluded from the table

Table 4 *P* values depicting virtual monoenergetic arterial images with significantly higher CNR compared to true arterial phase images

Arterial segment	40 keV	45 keV	50 keV	55 keV
Venous phase monoenergy values with significantly higher CNR compared to arterial phase				
R carotid	0.12	0.59	0.9	1
L carotid	0.15	0.63	0.9	1
R subclavian	0.10	0.58	0.9	1
L subclavian	0.10	0.56	0.9	1
Brachiocephalic	0.06	0.51	0.9	1
Asc thoracic aorta	0.03	0.33	0.8	1
Aortic arch	0.01	0.20	0.7	1
Desc thoracic aorta	0.08	0.77	1	1
Suprarenal aorta	0.06	0.77	1	1
Celiac	0.14	0.86	1	1
Superior mesenteric	0.16	0.90	1	1
R renal	0.05	0.61	1	1
L renal	0.24	0.87	1	1
Infrarenal aorta	< 0.001	0.02	0.61	1
R common iliac	< 0.001	0.00	0.17	0.82
L common iliac	< 0.001	0.00	0.09	0.67
R external iliac	< 0.001	0.01	0.29	0.92
L external iliac	< 0.001	0.00	0.12	0.76

All *P* values at 60 keV and beyond were statistically insignificant and excluded from the table

Conclusion

In summary, SDCT can create virtual monoenergetic arterial images from a venous phase CTA that have equivalent and in some cases significantly higher SNR and CNR of aortoiliac arteries than the true arterial phase, similar to studies examining DECT but without the need for prospective patient selection. Further investigation is needed to establish the clinical applicability of SDCT in vascular imaging.

Compliance with Ethical Standards

Conflict of interest The authors declare that they have no conflict of interest.

Ethical Approval All procedures performed in studies involving human participants were in accordance with the ethical standards of the institutional and/or national research committee and with the 1964 Helsinki declaration and its later amendments or comparable ethical standards. This article does not contain any studies with animals performed by any of the authors.

Informed Consent Informed consent was obtained from all individual participants included in the study.

References

1. Ananthakrishnan L, Rajiah P, Ahn R, et al. Spectral detector CT-derived virtual non-contrast images: comparison of attenuation values with unenhanced CT. Abdom Radiol (NY). 2017;42(3):702–9.
2. McCollough CH, Leng S, Yu L, Fletcher JG. Dual- and multi-energy CT: principles, technical approaches, and clinical applications. Radiology. 2015;276(3):637–53.
3. Rajiah P, Abbara S, Halliburton SS. Spectral detector CT for cardiovascular applications. Diagn Interv Radiol. 2017;23(3):187–93.
4. Kalva SP, Sahani DV, Hahn PF, Saini S. Using the K-edge to improve contrast conspicuity and to lower radiation dose with a 16-MDCT: a phantom and human study. J Comput Assist Tomogr. 2006;30(3):391–7.
5. Coursey CA, Nelson RC, Boll DT, et al. Dual-energy multidetector CT: how does it work, what can it tell us, and when can we use it in abdominopelvic imaging? Radiographics. 2010;30(4):1037–55.
6. Machida H, Tanaka I, Fukui R, et al. Dual-energy spectral CT: various clinical vascular applications. Radiographics. 2016;36(4):1215–32.
7. Beeres M, Trommer J, Frellesen C, et al. Evaluation of different keV-settings in dual-energy CT angiography of the aorta using advanced image-based virtual monoenergetic imaging. Int J Cardiovasc Imaging. 2016;32(1):137–44.
8. Boos J, Fang J, Heidinger BH, Raptopoulos V, Brook OR. Dual energy CT angiography: pros and cons of dual-energy metal artifact reduction algorithm in patients after endovascular aortic repair. Abdom Radiol (NY). 2017;42(3):749–58.
9. Chandarana H, Godoy MC, Vlahos I, et al. Abdominal aorta: evaluation with dual-source dual-energy multidetector CT after endovascular repair of aneurysms–initial observations. Radiology. 2008;249(2):692–700.
10. Flors L, Leiva-Salinas C, Norton PT, Patrie JT, Hagspiel KD. Endoleak detection after endovascular repair of thoracic aortic aneurysm using dual-source dual-energy CT: suitable scanning protocols and potential radiation dose reduction. AJR Am J Roentgenol. 2013;200(2):451–60.
11. Flors L, Leiva-Salinas C, Norton PT, Patrie JT, Hagspiel KD. Imaging follow-up of endovascular repair of type B aortic dissection with dual-source, dual-energy CT and late delayed-phase scans. J Vasc Interv Radiol. 2014;25(3):435–42.
12. Maturen KE, Kaza RK, Liu PS, Quint LE, Khalatbari SH, Platt JF. "Sweet spot" for endoleak detection: optimizing contrast to noise using low keV reconstructions from fast-switch kVp dual-energy CT. J Comput Assist Tomogr. 2012;36(1):83–7.
13. Numburi UD, Schoenhagen P, Flamm SD, et al. Feasibility of dual-energy CT in the arterial phase: imaging after endovascular aortic repair. AJR Am J Roentgenol. 2010;195(2):486–93.
14. Sommer WH, Graser A, Becker CR, et al. Image quality of virtual noncontrast images derived from dual-energy CT angiography after endovascular aneurysm repair. J Vasc Interv Radiol. 2010;21(3):315–21.
15. Stolzmann P, Frauenfelder T, Pfammatter T, et al. Endoleaks after endovascular abdominal aortic aneurysm repair: detection with dual-energy dual-source CT. Radiology. 2008;249(2):682–91.
16. De Cecco CN, Schoepf UJ, Steinbach L, et al. White paper of the society of computed body tomography and magnetic resonance on dual-energy CT, part 3: vascular, cardiac, pulmonary, and musculoskeletal applications. J Comput Assist Tomogr. 2017;41(1):1–7.
17. Albrecht MH, Scholtz JE, Husers K, et al. Advanced image-based virtual monoenergetic dual-energy CT angiography of the abdomen: optimization of kiloelectron volt settings to improve image contrast. Eur Radiol. 2016;26(6):1863–70.
18. Pinho DF, Kulkarni NM, Krishnaraj A, Kalva SP, Sahani DV. Initial experience with single-source dual-energy CT abdominal angiography and comparison with single-energy CT angiography: image quality, enhancement, diagnosis and radiation dose. Eur Radiol. 2013;23(2):351–9.
19. Yin XP, Zuo ZW, Xu YJ, et al. The optimal monochromatic spectral computed tomographic imaging plus adaptive statistical iterative reconstruction algorithm can improve the superior mesenteric vessel image quality. Eur J Radiol. 2017;89:47–53.
20. Sudarski S, Apfaltrer P, Nance JW Jr, et al. Optimization of keV-settings in abdominal and lower extremity dual-source dual-energy CT angiography determined with virtual monoenergetic imaging. Eur J Radiol. 2013;82(10):e574–81.
21. Wichmann JL, Gillott MR, De Cecco CN, et al. Dual-energy computed tomography angiography of the lower extremity runoff: impact of noise-optimized virtual monochromatic imaging on image quality and diagnostic accuracy. Invest Radiol. 2016;51(2):139–46.
22. Lee J, Park CH, Oh CS, Han K, Kim TH. Coronary computed tomographic angiography at 80 kVp and knowledge-based iterative model reconstruction is non-inferior to that at 100 kVp with iterative reconstruction. PLoS ONE. 2016;11(9):e0163410.
23. The 2007 recommendations of the International Commission on Radiological Protection. ICRP publication 103. Ann ICRP. 2007;37(2–4):1–332.